Paper:

Study on Infrared Transmittance of Si-Polymer Hybrid Structure Press Molded Using a Coupling Agent

Hibiki Ishide and Jiwang Yan[†]

Department of Mechanical Engineering, Faculty of Science and Technology, Keio University
3-14-1 Hiyoshi, Kohoku-ku, Yokohama, Kanagawa 223-8522, Japan
[†]Corresponding author, E-mail: yan@mech.keio.ac.jp
[Received June 27, 2019; accepted September 3, 2019]

Hybrid structures of single-crystal silicon and high-density polyethylene (HDPE) with high transmittance in the mid-to-far infrared region are used as infrared lens substrates. The hybrids are usually fabricated by high-precision press molding. The Si-HDPE hybrid lens previously fabricated had a low transmittance in the 9–10 μm wavelength region, thereby limiting its application for human body detection. In this study, a Si-polymer hybrid structure was fabricated using a new polymer without any silane coupling agent. Interfacial adhesion between the polymer and the Si substrate was realized with an extremely thin (a few micron thick) layer of an interfacial silane coupling agent. The press molding conditions that led to improved bonding strength and infrared transmittance of the hybrid substrate were investigated. A transmittance similar to that of a single-crystal Si substrate was achieved in the 9–10 μm wavelength range.

Keywords: infrared lens, silicon, polymer, press molding, hybrid optics

1. Introduction

There is a considerable demand for infrared (IR) optical systems due to their wide range of applications such as security surveillance, rescuing in darkness, assisting drivers at night, and thermography. The major challenges in the mass production of IR lenses are decreasing the size and weight of the lens and reducing the manufacturing costs, which can result in cheaper IR cameras. Hence, new fabrication methods for IR lenses that can overcome these challenges are required [1, 2].

Ge, Si, zinc selenide, chalcogenide glasses, etc. are the materials mainly used in IR optics [3–5]. In particular, Ge and Si are widely used for the fabrication of IR lenses because of their excellent IR properties (IR transmittance, refractive index, etc.) in the mid-to-far IR region [1]. In recent years, semiconductors have been ductile machined into aspherical or Fresnel IR lenses by ultra-precision diamond turning or grinding without subsequent polishing. However, these machining processes are expensive and time consuming because of the hard and brittle nature of Ge and Si, resulting in severe tool wear and a very high production cost. Thus, for the mass production of IR optical materials, an alternative fabrication method is required.

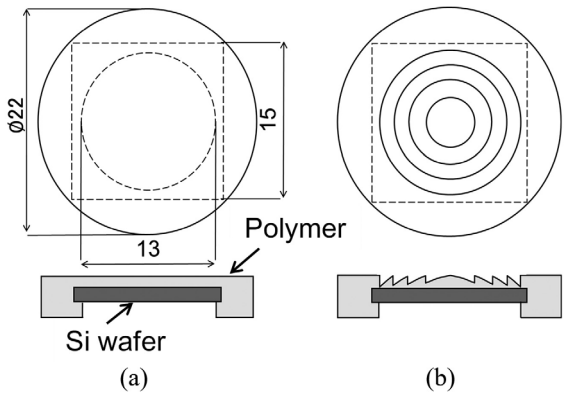

Fig. 1. Design of (a) hybrid substrate and (b) hybrid lens.

In our previous work, a novel method based on press molding was developed for the manufacture of hybrid IR lenses [1]. In this method, a hybrid structure of single-crystal Si and high-density polyethylene (HDPE) were press molded. The structure of the Si-HDPE hybrid substrate is shown in **Fig. 1**. A double-sided polished Si wafer was laminated with a thin film of HDPE, which had high transmittance in the mid-to-far IR region [6]. During the press molding process, they were mechanically locked by compression. The two materials were bonded, and the Fresnel lens shape was transferred onto the surface of HDPE by press molding. Notably, in this method, the fragile Si substrate is protected from external shocks by HDPE. In addition, the flatness of the HDPE film can be maintained by the high-stiffness Si substrate, and there is no need to machine the Si substrate itself [1]. Furthermore, the Si-HDPE hybrid lens can be fabricated in a considerably shorter time by this method as compared to conventional machining. Moreover, the polymer material enables the transfer of complicated shapes in mass production [7]. Thus, this method can facilitate low-cost mass production of IR lenses.

However, the Si-HDPE hybrid lens fabricated by this method has a limitation: lower transmittance in the

Table 1. Si material properties.

Thickness [μm]	780
Refractive index	3.5 (1.5–11 μm)
Surface roughness *Ra* [nm]	3.5
Shape	Square
Size [mm]	15×15

9–10 μm wavelength region than that of Si. According to Wien's displacement law, the IR radiation peak from the human body lies in this wavelength region. Therefore, a low transmittance in this region considerably affects human body detection. The low transmittance is caused by silane coupling agents present in HDPE, which is used as the lens material. Silane coupling agents are utilized as adhesion promoters between organic, inorganic, or metallic components [8, 9]. However, their IR absorbance in the 9–10 μm wavelength region is high because of stretching bond vibrations caused by molecular chains in the system [10–17].

In this study, a Si-polymer hybrid with improved IR transmittance in the 9–10 μm wavelength region was fabricated with a new polymer, without any silane coupling agent. The IR transmittance loss was suppressed by using an extremely small amount of a silane coupling agent only at the interface between Si and the polymer. In addition, the material characteristics and IR transmittance of the hybrid substrate were investigated in this work.

2. Experimental Procedures

2.1. Sample Materials

Two materials were mainly used for the hybrid lens fabrication. The first one was a two-side polished Si wafer with 780 μm thickness, cut into a 15 mm square using a diamond pen. The Si wafer was used as the hybrid lens substrate. The material properties of the Si wafer are presented in **Table 1**. For the polymer layer of the hybrid lens, a new polymer without any silane coupling agent (POLY IR® 9, Fresnel Technologies, Inc., USA) was used. In addition, HDPE (LINKLON HM600A, Mitsubishi Chemical Corporation, Japan), a silane crosslinkable resin, was used for comparison. HDPE is labeled as polymer A and the new polymer, POLY IR® 9, is labeled as polymer B in this paper. The material properties of these polymers are given in **Table 2**. A comparison of the IR transmittance of the two polymers is shown in **Fig. 2**; the transmittance was measured at a polymer thickness of 380 μm. The transmittance of polymer B in the 9–10 μm wavelength region is higher than that of polymer A because of the absence of the silane coupling agent.

2.2. Press Molding Process and Conditions

Figure 3 illustrates the fabrication of the hybrid structure by the press molding process. The Si wafer was

Table 2. Material properties of polymers A and B.

	Polymer A	Polymer B
Material name	HDPE	POLY IR® 9
Melting point [°C]	129.5	132.5
Refractive index	1.5 (8.5–12 μm)	1.54 (8–14 μm)
Shape	Granule	Square
Size [mm]	$\phi 3 \times 3.5$	15×15

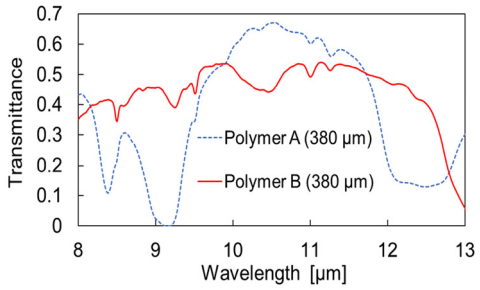

Fig. 2. Comparison of IR transmittance of polymer A and polymer B.

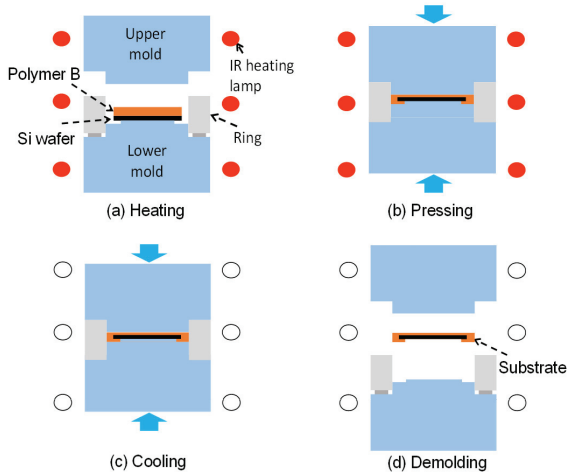

Fig. 3. Schematic diagram of press molding process: (a) heating, (b) pressing, (c) cooling, and (d) demolding.

placed inside the mold cavity along with the polymer. Then, the lower mold was raised towards the upper mold and the material was heated with the circular IR lamps surrounding the molds. During the press molding process, the two molds were closed and compression was started after the temperature reached the melting point of the polymer. A ring spacer was used to adjust the mold closing position. The thickness of the polymer layer on the Si wafer was controlled by controlling the molding temperature and the pressing load. During heating, the polymer laminated and enclosed the Si wafer. The molds were then allowed to cool down, and they were opened after the cooling ended.

The hybrid substrate was fabricated using a high-

Table 3. Press molding conditions at different temperatures.

Heating temperature [°C]	150, 160, 180, 200, 220, 240
Pressing force [kN]	0.3
Cooling temperature [°C]	90
Pressing time [min]	5

Table 4. Press molding conditions at different pressing forces.

Heating temperature [°C]	180
Pressing force [kN]	0.5, 1.0, 1.5
Cooling temperature [°C]	90
Pressing time [min]	5

precision glass molding machine, GMP 211 (Toshiba Machine Co., Ltd., Japan). The heating temperature was increased up to 800°C, with ±1°C accuracy. The pressing force was in the range of 0.2–20 kN with a resolution of 0.98 N. To prevent oxidation of the sample, press molding was performed in an argon gas atmosphere.

In this work, hybrid substrates were fabricated under various heating temperatures and pressing forces. The press molding conditions at different heating temperatures and pressing forces are listed in **Tables 3** and **4**, respectively. Furthermore, the adhesion state between the Si wafer and polymer, with and without the silane coupling agent, was compared.

2.3. IR Transmittance Measurement

The IR transmittance of the hybrid substrates fabricated at different conditions was measured with a Fourier-transform IR (FTIR) spectrometer. This instrument could measure IR transmittance and absorbance in the wavelength range from 2.5 μm to 25 μm. During the measurement, the sample was placed between the IR source and the detector. In this study, the measurement was performed in the 8–13 μm wavelength region (i.e., the range in which IR cameras detect the human body).

3. Results and Discussion

3.1. IR Transmittance Comparison

Figure 4 shows the comparison of the IR transmittance of the hybrid substrate containing polymer B without any silane coupling agent at different heating temperatures. The thicknesses of the polymers after press molding are shown in the legends in the graph. The IR transmittance increased with an increase in the heating temperature from 160°C to 180°C. This improvement was attributed to the fact that the viscosity of polymer B decreased with increasing temperature and the polymer became thinner. However, a further increase in the temperature did not improve the transmittance even though the polymer thickness was low. At high heating temperatures, over 180°C, thermally induced degradation of the polymer might have occurred. However, at heating temperatures below 150°C, the polymer did not laminate and properly enclose the Si substrate because of low fluidity. Therefore, for the polymer to laminate and properly enclose the Si substrate, it has to be heated at a temperature higher than the melting point, which leads to decreased viscosity. Based on these results, it was found that the optimum heating temperature to achieve high IR transmittance for the hybrid substrate was 180°C. **Fig. 5** shows the comparison of the IR transmittance for different pressing forces; the thicknesses of the polymers after press molding are shown in the legends. Although higher pressing forces resulted in a higher IR transmittance, cracks were formed at the bottom surface of the Si wafer at 1.5 kN because the pressing force was considerably high. Therefore, the optimum pressing force to maintain bonding between Si and the polymer with high IR transmittance was 1.0 kN.

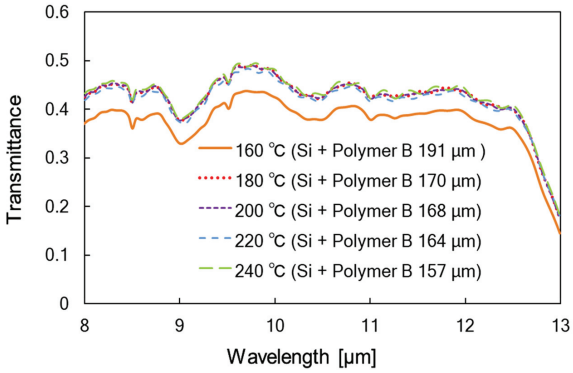

Fig. 4. IR transmittance at different heating temperatures.

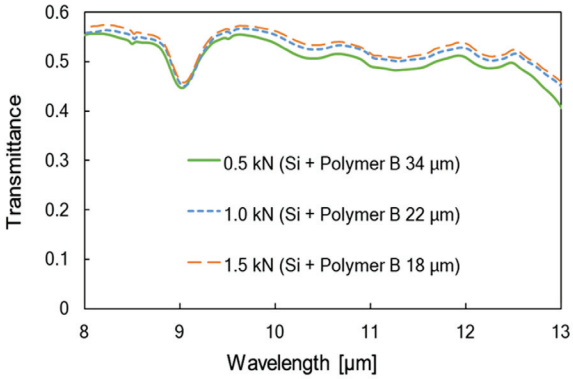

Fig. 5. IR transmittance at different pressing forces.

3.2. Thermal Effect on Polymer Structure

Not only the thickness of the polymer after press molding, but also crystallization of the polymer during heating could affect the IR transmittance. **Fig. 6** shows a schematic of polymer crystallization. A crystalline polymer normally consists of two different parts: crystalline regions, where the molecular chains are orderly arranged,

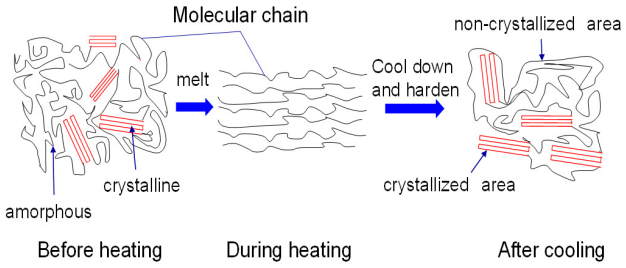

Fig. 6. Schematic of polymer crystallization.

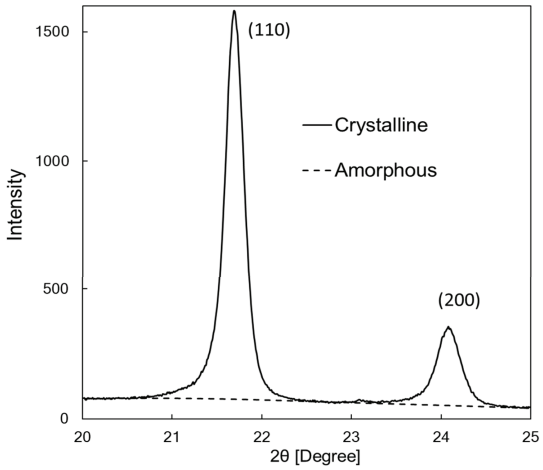

Fig. 7. XRD pattern of polymer B at a temperature of 160°C.

and amorphous regions, where the molecular chains are randomly tangled. As shown in **Fig. 6**, when the polymer is heated, the molecular chains become untangled. After cooling and hardening, some areas crystallize while others become amorphous. Crystallization is dependent on the cooling rate. According to previous research, the higher the cooling rate, the lower is the final degree of crystallinity [18].

In previous studies, it was determined that IR transmittance is also affected by IR absorbance, which is caused by molecular bonding vibrations [1]. In the crystallized regions, molecular vibrations are restricted; accordingly, the IR absorbance of the polymer decreases with an increase in the proportion of the crystallized region. Therefore, enhanced crystallization of the polymer results in improved IR transmittance.

In this study, the polymer crystallinity was measured by X-ray diffraction (XRD), which is widely used for determining the degree of crystallinity [19–23]. The XRD pattern of polymer B at a heating temperature of 160°C is shown in **Fig. 7**. As shown in this pattern, sharp peaks were observed between 21° and 22° and at around 24°. The first peak was assigned to the (110) reflection of the crystalline plane and the second peak was assigned to the (200) reflection of the crystalline plane [24–26]. The solid line represents the crystalline phase and the dashed line represents the amorphous phase. From the separation between the peaks of the two phases, the degree of crystallinity of the polymer was determined using Eq. (1):

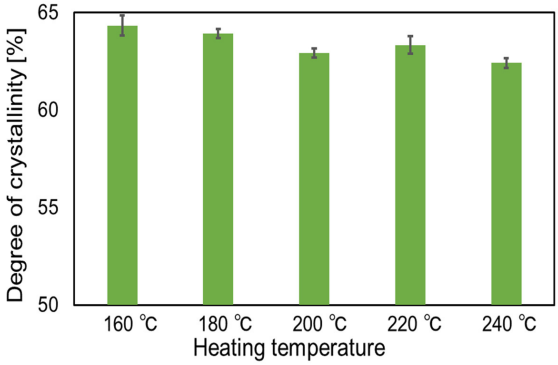

Fig. 8. Degree of crystallinity in polymer B at different heating temperatures.

$$X_C\,[\%] = \frac{I_C}{I_A + I_C} \times 100, \quad \ldots\ldots\ldots\ldots \quad (1)$$

where I_A and I_C are the integrations of scattered intensities for the amorphous and crystalline peaks, respectively. **Fig. 8** shows the degrees of crystallinity of the polymer samples heated at different temperatures, calculated using Eq. (1) in the 20–25° range. The error bars in **Fig. 8** are standard deviations of every five measurements.

As shown in **Fig. 8**, the degree of crystallinity decreased with increasing heating temperature. After cooling, a higher proportion of the amorphous region was formed in the polymer at a higher heating temperature, because the molecular chains were not orderly arranged. In the amorphous regions, the IR absorbance was higher because of molecular vibrations. On the other hand, in the crystalline regions, the vibrations were suppressed. Therefore, the IR absorbance increased with increasing heating temperature, which resulted in the formation of more amorphous regions.

3.3. Polymer Surface Observation

To investigate the surface topography of the polymer after cooling from different heating temperatures, SEM was conducted and the images are shown in **Fig. 9**. For all conditions, some complex wrinkles were observed in the micrographs. In addition, the number of wrinkles increased with increasing heating temperature. These wrinkles were caused by shrinkage during the cooling process. A higher heating temperature corresponded to a longer cooling time, which led to the formation of more wrinkles.

3.4. Polymer Surface Measurement

To compare the surfaces of the polymer samples under each pressing condition, surface roughness was measured with a laser microscope, as shown in **Fig. 10**. To improve the reliability of the measurement, 20 areas on each sample were measured and the average was taken. Typically, the measurement was performed on a 645 × 645 μm^2

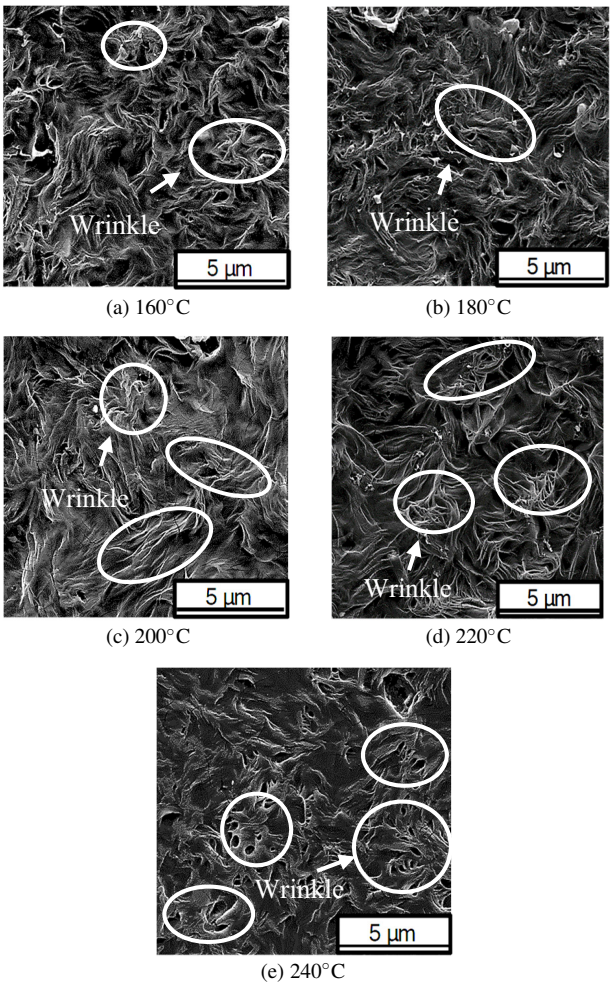

(a) 160°C (b) 180°C (c) 200°C (d) 220°C (e) 240°C

Fig. 9. SEM images of polymer surfaces at different temperatures.

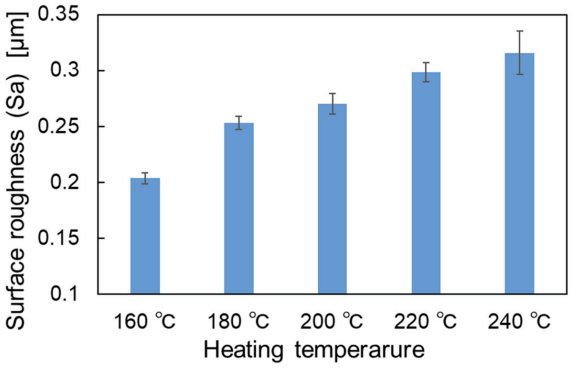

Fig. 10. Surface roughness of polymer samples at different heating temperatures.

square with cutoff lengths λ_c, λ_s, and λ_f of 80 μm using a lens with a magnification of 20 (NA: 0.60). As seen in **Fig. 10**, the surface roughness increased with increasing heating temperature. According to previous research, an increase in the surface roughness causes a decrease in the transmittance [27]. This might be the reason why the IR transmittance did not improve even when the polymer layer thickness was low at high heating temperatures (**Fig. 4**). The effect of surface roughness increase almost cancels the effect of polymer thickness reduction. It is considered that the increase in the surface roughness is caused by shrinkage during the cooling process. Shrinkage occurs due to thermal contraction during cooling [28–30]; accordingly, a high heating temperature results in enhanced shrinkage, because of a longer cooling time [31].

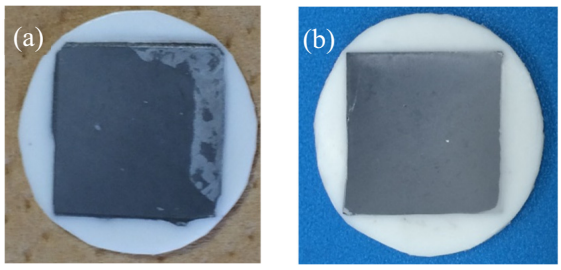

Fig. 11. Hybrid substrate molded (a) without and (b) with silane coupling agent at the interface.

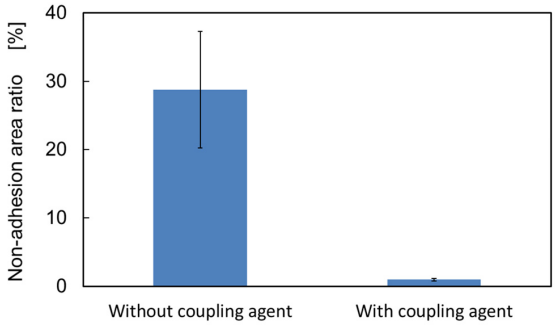

Fig. 12. Comparison of non-adhesion area ratio.

3.5. Effect of Silane Coupling Agent on Interfacial Adhesion

Optimal heating temperature and pressing force were applied during the fabrication of the hybrid substrates. However, as shown in **Fig. 11(a)**, for the hybrid substrate without any interfacial silane coupling agent, unadhered areas between the Si wafer and polymer B were observed. This was attributed to the low adhesive property of the crystalline polymer. To solve this problem, an extremely thin layer ($\sim$6 μm) of a silane coupling agent was introduced at the interface between the Si wafer and polymer. A compatibilizer between inorganic fillers and organic polymers, vinyl trimethoxy silane (Dynasylan 6490, Evonik Degussa Japan Co., Ltd.), was used as the coupling agent. The coupling agent was added at 1% (by volume of the wafer, 0.0013 g) on the wafer and then heated at 200°C for 30 min. Subsequently, the unadhered area disappeared after press molding, as shown in **Fig. 11(b)**.

Figure 12 shows the comparison of the unadhered area ratio for substrates with and without the coupling agent. With the silane coupling agent, the unadhered area could be reduced by approximately 97%. **Fig. 13** shows the

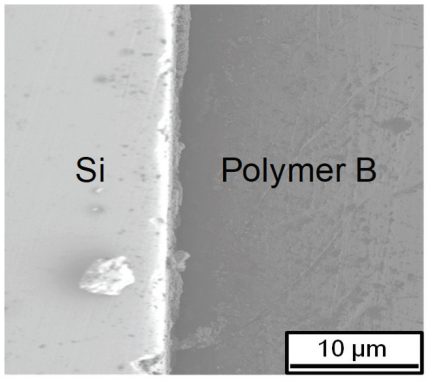

Fig. 13. SEM image of the interface between Si and polymer B.

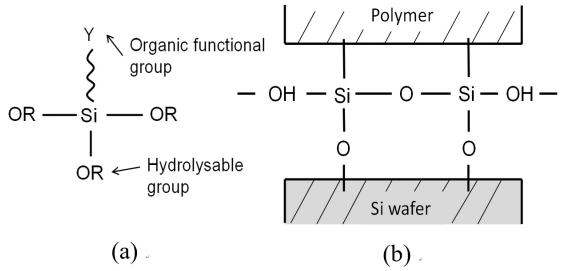

Fig. 14. (a) Molecular structure of silane coupling agent and (b) coupling structure between Si and polymer.

SEM image of the interface between Si and the polymer with the coupling agent. No gap was observed between the surfaces. Thus, the application of the silane coupling agent resulted in improved interfacial adhesion between the Si wafer and polymer B in the hybrid substrate.

Figure 14 shows the molecular structure of the silane coupling agent and the coupling structure between the Si wafer and polymer. The silane coupling agent consists of two functional groups: a hydrolysable group and an organic functional group. In the presence of water, in air, the hydrolyzable group is hydrolyzed and becomes an active silanol group. The silanol group reacts with the inorganic filler via the Si-O bond, resulting in condensation (lower part of **Fig. 14(b)**). Alternatively, in the presence of a radical, the organic functional group reacts with the unsaturated double bond of the polymer or radical polymer (upper part of **Fig. 14(b)**). Thus, via these mechanisms, the Si wafer and polymer B were firmly bonded.

3.6. Effect of Silane Coupling Agent on IR Transmittance

Figure 15 shows the IR transmittance spectra of hybrid substrates with and without the interfacial silane coupling agent; the thicknesses of the polymer layers after press molding are given in the legends. For comparison, the spectrum of the hybrid substrate obtained using polymer A and Si is also included in **Fig. 15**. The IR transmittance of Si-polymer B hybrid substrates with and without the silane coupling agent was higher than that of

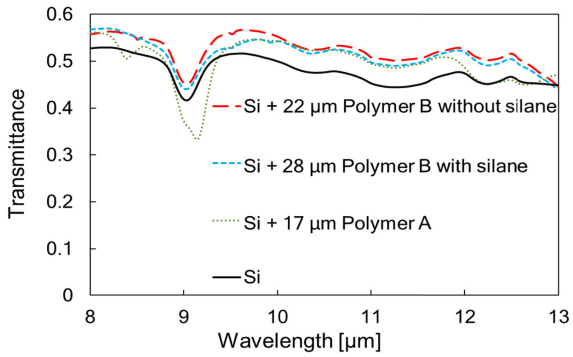

Fig. 15. IR transmittance spectra of Si-polymer B hybrid substrates without and with the interfacial silane coupling agent, Si-polymer A hybrid substrate, and Si.

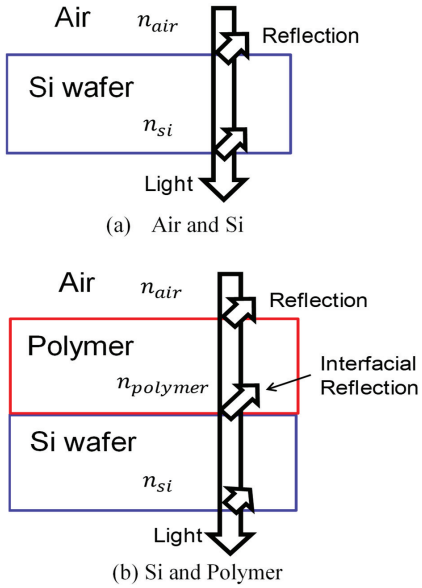

Fig. 16. Mechanism of light reflection at the interface between two materials of cases (a) and (b).

the Si-polymer A hybrid substrate in the 9–10 μm wavelength region. In addition, the IR transmittance of the substrate with the agent was slightly lower than that without the agent, particularly in the 9–10 μm wavelength region. This was attributed to the IR absorbance of the silane coupling agent. However, the IR transmittance of all hybrid substrates was higher than that of Si. This was attributed to a lower interfacial reflection between Si and the polymer, as shown in **Fig. 16**. According to Fresnel's law, a difference in the refractive index between two materials causes a decrease in the interfacial reflection R (n_a and n_b are the refractive indexes of materials A and B), as shown in Eq. (2).

$$R = \left| \frac{n_a - n_b}{n_a + n_b} \right|^2 \quad \cdots\cdots\cdots\cdots\cdots\cdots \quad (2)$$

In the case of only Si, interfacial reflection occurred between air and Si. The refractive index difference was 2.5 and R was 0.31 (calculated from Eq. (2)). On the other

hand, the refractive index difference between Si and polymer A was 1.9 and that between Si and polymer B was 1.96. Notably, R ($\sim$0.16) calculated from Eq. (2) was smaller than that for only Si. This was the reason for the lower interfacial reflection in the case of Si and polymer than that for only Si. Accordingly, the IR transmittance of the hybrid substrates was higher than that of Si. Thus, the hybrid substrate obtained using polymer B exhibited high IR transmittance (sufficiently high for IR hybrid lenses) although it contained an interfacial silane coupling agent.

4. Conclusions

To obtain a hybrid IR lens with improved IR transmittance, a new polymer without any coupling agent was press molded onto Si. The characteristics and the IR transmittance of the hybrid substrates were investigated. The main conclusions are summarized as follows.

1. The optimal heating temperature and pressing force for improved IR transmittance were 180°C and 1.0 kN.

2. The Si-polymer B hybrid substrate showed superior IR transmittance in the wavelength range of 9–10 μm as compared to Si-polymer A and Si.

3. The IR transmittance of the hybrid substrates was affected by the crystallinity of the polymer.

4. The surface roughness of the polymer varied with the heating conditions, which also affected the IR transmittance.

5. The IR transmittance of the hybrid substrate was improved by using an extremely thin layer ($\sim$6 μm) of a silane coupling agent at the interface of Si-polymer B.

References:

[1] A. R. A. Manaf and J. Yan, "Press molding of a Si-HDPE hybrid lens substrate and evaluation of its infrared optical properties," Precision Engineering, Vol.43, pp. 429-438, 2016.

[2] A. R. A. Manaf, T. Sugiyama, and J. Yan, "Design and fabrication of Si-HDPE hybrid Fresnel lenses for infrared imaging systems," Optics Express, Vol.25, Issue 2, pp. 1202-1220, 2017.

[3] R. A. Soref, S. J. Emelett, and W. R. Buchwald, "Silicon waveguided components for the long-wave infrared region," J. of Optics A: Pure and Applied Optics, Vol.8, pp. 840-848, 2006.

[4] L. Shen, N. Healy, C. J. Mitchell, J. S. Penades, M. Nedeljkovic, G. Z. Mashanovich, and A. C. Peacock, "Mid-infrared all-optical modulation in low-loss germanium-on-silicon waveguides," Optics Letters, Vol.40, Issue 2, pp. 268-271, 2015.

[5] T. Grulois, G. Druart, N. Guérineau, A. Crastes, H. Sauer, and P. Chavel, "Extra-thin infrared camera for low-cost surveillance applications," Optics Letters, Vol.39, Issue 11, pp. 3169-3172, 2014.

[6] N. E. Claytor and R. N. Claytor, "Polymer Imaging Optics for the Thermal Infrared," Proc. of SPIE, Vol.5406, pp. 107-113, 2004.

[7] Y. Murata and M. Kuramochi, "Development of Heating and Cooling Injection Mold with Far-Infrared Radiation Heater," Int. J. Automation Technol., Vol.10, No.1, pp. 79-86, 2016.

[8] Y. Xie, C. A. S. Hill, Z. Xiao, H. Militz, and C. Mai, "Silane coupling agents used for natural fiber/polymer composites," Composites Part A: Applied Science and Manufacturing, Vol.41, pp. 806-819, 2010.

[9] M. Hashizume, S. Fukagawa, S Mishima, T. Osuga, and K. Iijima, "Hot-Press-Assisted Adhesions between Polyimide Films and Titanium Plates Utilizing Coating Layers of Silane Coupling Agents," Langmuir, Vol.32, No.47, pp. 12344-12351, 2016.

[10] A. Valadez-Gonzalez, J. M. Cervantes-Uc, R. Olayo, and P. J. Herrera-Franco, "Chemical modification of henequén fibers with an organosilane coupling agent," Composites Part B: Engineering, Vol.30, pp. 321-331, 1999.

[11] D. I. Tee, M. Mariatti, A. Azizan, C. H. See, and K. F. Chong, "Effect of silane-based coupling agent on the properties of silver nanoparticles filled epoxy composites," Composites Science and Technology, Vol.67, pp. 2584-2591, 2007.

[12] J. Kim, D. Lee, T. Oh, and D. Lee, "Characteristics of Nitrile-Butadiene Rubber Layered Silicate Nanocomposites with Silane Coupling Agent," J. of Applied Polymer Science, Vol.89, Issue 10, pp. 2633-2640, 2003.

[13] J. P. Matinlinna, K. Laajalehto, T. Laiho, I. Kangasniemi, L. V. J. Lassila, and P. K. Vallittu, "Surface analysis of Co-Cr-Mo alloy and Ti substrates silanized with trialkoxysilanes and silane mixtures," Surface and Interface Analysis, Vol.36, Issue 3, pp. 246-253, 2004.

[14] G. S. Ahmed, M. Gilbert, S. Mainprize, and M. Rogerson, "FTIR analysis of silane grafted high density polyethylene," Plastics, Rubber and Composites, Vol.38, No.1, pp. 13-20, 2009.

[15] C. Rosales, R. Perera, M. Ichazo, J. Gonzalez, H. Rojas, A. Sanchez, and A. Díaz Barrios, "Grafting of Polyethylenes by Reactive Extrusion. I. Influence on the Molecular Structure," J. of Applied Polymer Science, Vol.70, pp. 161-176, 1998.

[16] Y. T. Shieh and T. H. Tsai, "Silane Grafting Reactions of Low-Density Polyethylene," J. of Applied Polymer Science, Vol.69, pp. 255-261, 1998.

[17] K. Sirisinha, M. Boonkongkaew, and S. Kositchaiyong, "The effect of silane carriers on silane grafting of high-density polyethylene and properties of crosslinked products," Polymer Testing, Vol.29, Issue 8, pp. 958-965, 2010.

[18] P. Sajkiewicz, A. Wasiak, A. Wozniak, and A. Woźniak, "Effects of cooling rate on crystallinity of i-polypropylene and polyethylene terephthalate crystallized in nonisothermal conditions," J. of Polymer Science Part B: Polymer Physics, Vol.37, Issue 20, pp. 2821-2827, 1999.

[19] T. Volke-Sepulveda, G. Saucedo-Casraneda, M. Gutierrez-Rojas, A. Manzur, and E. Favela-Torres, "Thermally Treated Low Density Polyethylene Biodegradation By Penicillium Pinophilum and Aspergillus Niger," J. of Applied Polymer Science, Vol.83, Issue 2, pp. 305-314, 2001.

[20] S. H. Han, Y. S. Yeom, J. G. Ko, H. C. Kang, and H. G. Yoon, "Effect of the degree of crystallinity on the electrical properties of MWCNT filled poly (ethylene-co-ethyl acrylate)/LDPE blend composites prepared by melt mixing," Composites Science and Technology, Vol.117, pp. 351-356, 2015.

[21] G. Trovati, E. A. Sanches, S. C. Neto, Y. P. Mascarenhas, and G. O. Chierice, "Characterization of Polyurethane Resins by FTIR, TGA, and XRD," J. of Applied Polymer Science, Vol.115, pp. 263-268, 2010.

[22] R. Ricciardi, F. Auriemma, C. D. Rosa, and F. Laupretre, "X-ray Diffraction Analysis of Poly(vinyl alcohol) Hydrogels, Obtained by Freezing and Thawing Techniques," Macromolecules, Vol.37, Issue 5, pp. 1921-1927, 2004.

[23] K. Toba, H. Yamamoto, and M. Yoshida, "Crystallization of cellulose microfibrils in wood cell wall by repeated dry-and-wet treatment, using X-ray diffraction technique," Cellulose, Vol.20, Issue 2, pp. 633-643, 2013.

[24] A. M. Youssef, A. El-Gendy, and S. Kamel, "Evaluation of corn husk fibers reinforced recycled low density polyethylene composites," Materials Chemistry and Physics, Vol.152, pp. 26-33, 2015.

[25] M. Munaro and L. Akcelrud, "Correlations between composition and crystallinity of LDPE/HDPE blends," J. of Polymer Research, Vol.15, Issue 1, pp. 83-88, 2008.

[26] G. Matsuba, K. Shimizu, H. Wang, Z. Wang, and C. C. Han, "Kinetics of phase separation and crystallization in poly(ethylene-ran-hexene) and poly(ethylene-ran-octene)," Polymer, Vol.44, Issue 24, pp. 7459-7465, 2003.

[27] A. Larena, F. Millan, G. Perez, and G. Pinto, "Effect of surface roughness on the optical properties of multilayer polymer films," Applied Surface Science, Vol.187, Issues 3-4, pp. 339-346, 2002.

[28] H. Hassan, N. Regnier, C. Pujos, E. Arquis, and G. Defaye, "Modeling the effect of cooling system on the shrinkage and temperature of the polymer by injection molding," Applied Thermal Engineering, Vol.30, Issue 13, pp. 1547-1557, 2010.

[29] S. Fathi and A. H. Behravesh, "Visualization of in-mold shrinkage in injection molding process," Polymer Engineering and Science, Vol.47, Issue 5, pp. 750-756, 2007.

[30] Y. Liu and M. Gehde, "Effects of surface roughness and processing parameters on heat transfer coefficient between polymer and cavity wall during injection molding," The Int. J. of Advanced Manufacturing Technology, Vol.84, Issues 5-8, pp. 1325-1333, 2016.
[31] T. C. Chang, "Shrinkage behavior and optimization of injection molded parts stuided by the Taguchi method," Polymer Engineering and Science, Vol.41, Issue 5, pp. 703-710, 2001.

Name:
Hibiki Ishide

Affiliation:
Graduate Student, Graduate School of Science and Technology, Keio University

Address:
3-14-1 Hiyoshi, Kohoku-ku, Yokohama, Kanagawa 223-8522, Japan

Brief Biographical History:
2018- Graduate School of Science and Technology, Keio University

Name:
Jiwang Yan

Affiliation:
Professor, Department of Mechanical Engineering, Faculty of Science and Technology, Keio University

Address:
3-14-1 Hiyoshi, Kohoku-ku, Yokohama, Kanagawa 223-8522, Japan

Brief Biographical History:
1987-1994 B.E./M.E. Candidate, Jilin University
1994-1996 Ph.D. Candidate, Tsinghua University
1996-2000 Ph.D. Candidate, Tohoku University
2000-2001 Research Associate, Tohoku University
2001-2005 Associate Professor, Kitami Institute of Technology
2005-2012 Associate Professor, Tohoku University
2012- Professor, Keio University

Main Works:
• ultraprecision machining, micro/nano manufacturing, material processing, and nanomechanics

Membership in Academic Societies:
• Japan Society of Mechanical Engineers (JSME)
• Japan Society for Precision Engineering (JSPE)
• Japan Society for Abrasive Technology (JSAT)
• Japan Society of Applied Physics (JSAP)
• American Society for Precision Engineering (ASPE)
• European Society for Precision Engineering and Nanotechnology (euspen)
• International Academy for Production Engineering (CIRP)